Preprint from Proceedings from the AVS International Symposium on Liquid Metal Processing and Casting, Santa Fe, New Mexico, February 16-19, 1997.

Anisotropic Porous Metals Production by Melt Processing

V. Shapovalov and L. Boiko

State Metallurgical Academy of Ukraine
Dnepropetrovsk, Ukraine

M. D. Baldwin, M. C. Maguire, and F. J. Zanner

Liquid Metal Processing Laboratory
Sandia National Laboratories
Albuquerque, New Mexico

Abstract

The collapse of the Soviet Union has left many of its scientific institutes and technical universities without their traditional backbone of financial support. In an effort to stem the export of science to nations advocating nuclear proliferation, and to acquire potentially useful technology, several U.S. government-sponsored programs have arisen to mine the best of former USSR scientific advances. In the field of metallurgy, the earliest institutes to be investigated by Sandia National Laboratories are located in Ukraine. In particular, scientists at the State Metallurgical Academy have developed unique porous metals, resembling what could be described as gas-solid "eutectic". While porous metals are available in the U.S. and other western countries, none have the remarkable structure and properties of these materials. Sandia began a collaborative program with the Ukrainian scientists to bring this technology to the U.S., verify the claims regarding these materials, and begin production of the so-called Gasars. This paper will describe the casting process technology and metallurgy associated with the production of Gasars, and will review the progress of the collaborative project.

This work was supported by the United States Department of Energy under contract DE-AC04-94AL85000. Sandia is multiprogram laboratory operated by Sandia Corporation, a Lockheed Martin Company, for the United States Department of Energy.

DISCLAIMER

Introduction

The recent change in relations between the former Soviet Union and the western countries has brought about some new and potentially exciting opportunities for collaborative research and development. In particular, insight into metallurgical processes used by the eastern bloc has generated considerable interest in the U.S. scientific community. With the goal of keeping nuclear and other weapons of mass destruction from reaching proliferant nations, the U.S. government is sponsoring several programs to foster joint research and development. These projects are meant to keep scientists and engineers in former Soviet countries, with their counterparts in this country, working to foster basic science or commercialize technology formerly used in weapons development. The metallurgical processes used in the former Soviet Union, while in most cases similar to western technology, sometimes showed some radical departures from common western processes. In the technology of metalcasting, the development of Anisotropic Porous Metals (APM) by Prof. V. Shapovalov at the State Metallurgical Academy of Ukraine in Dnepropetrovsk represents one of these previously unknown technologies to the West. The structure of these materials and the process used for their preparation has been termed Gasar.

Several techniques exist for production of porous or cellular metal structures. These include metal honeycombs, foamed structures, sintered metal powders, and several types of deposition processes. Most of these processes for porous metal preparation have been reviewed recently[1]. The distinction that materials produced by the Gasar process possess is that the geometry of the structure is driven by a solidification process. The pores grow along with the solidification interface giving rise to the often-used comparison to a eutectic structure, with the second phase being a gas rather than a solid. By manipulation of solidification conditions (usually with pressure, temperature, and thermal gradient) the pore structure can assume continuous or discontinuous geometries, a range of pore sizes and pore fractions, and a controllable shape of the final product.

The pores grow as a result of gas evolution, with hydrogen being the only reported gas used for this process[1]. While most efforts in the U.S. related to hydrogen in the metalcasting industry were generally associated with removing this deleterious gas, the Ukrainian approach was to charge the melt with hydrogen, generally under more than 1 atm pressure, and take advantage of its evolution as hydrogen gas during solidification. Figure 1 shows a series of schematic structures attainable with the Gasar process.

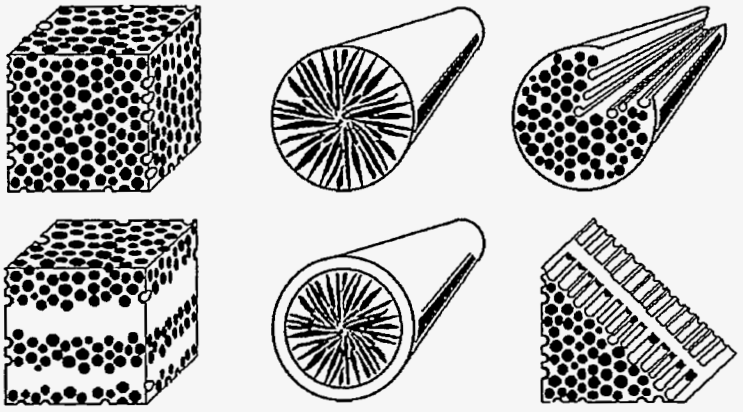

Figure 1. Schematic of Gasar structures reported by Shapovalov[1] with variations in solidification conditions. Pores align with solidification direction, and can be started and stopped with application of pressure.

Starting in 1993, Sandia National Laboratories began investigating these materials and their preparation. A collaborative project was initiated with DMK Tek, a U.S.-Ukrainian joint venture company that represents the Gasar inventor, Prof. Vladimir Shapovalov. The goals of this project were twofold. First, in order to determine if Gasar structures could be formed in

common U.S. high performance alloys, alloy-hydrogen phase diagrams were prepared for four alloys. These diagrams show the change in solubility of hydrogen when going from liquid to solid, a critical aspect of whether or not enough gas is evolved to generate significant porosity. Second, since results from the phase diagram determination were promising, a furnace capable of producing Gasar structures was jointly designed by Sandia and DMK Tek. The results of this project and the current status of U.S. capability to produce Gasar structures are reviewed in this paper.

Alloy Phase Diagrams

The four alloys chosen for phase diagram determination were Alloy 625, Alloy 718, ASTM F-75, and PH13-8Mo. The compositions of these alloys are shown in Table 1. The two nickel-base superalloys, Alloys 625 and 718, were chosen to evaluate whether Gasar structures were possible in the two most common alloys used in gas turbine and high temperature applications. The cobalt-base alloy ASTM F-75 is commonly used for biomedical implant applications where a porous metal structure may be of benefit. Finally, the precipitation hardening stainless steel PH13-8Mo was chosen because of its common application in weapon components by Sandia.. All materials have fairly complex chemistries for which no information existed regarding the effect of hydrogen on melting and solidification behavior. The procedures for determining the alloy-hydrogen phase diagrams were identical for each of the alloys. For purposes of brevity, the data acquired for the development of these diagrams will be illustrated for a single material, Alloy 625.

Table 1. Alloy Compositions Used in this Study

Element	Alloy 625	Alloy 718	ASTM F-75	PH13-8Mo
C	0.04	0.04	0.25	0.04
Mn	0.03	0.10	-	0.04
Si	0.08	0.16	-	0.04
P	0.004	0.005	-	0.005
S	0.002	0.0005	-	0.004
Cr	21.97	18.37	27	12.51
Mo	8.69	3.08	5	2.13
Ni	62.36	51.85	2.8	8.17
Co	0.04	0.62	Bal.	0.03
Al	0.16	0.66	-	1.11
Ti	0.25	1.00	-	0.014
Nb	3.89	5.16	-	-
Fe	2.50	18.67	-	Bal.
Cu	-	0.07	-	0.05
B	-	0.004	-	

The first step in the determination of the high temperature portion of the Alloy 625-hydrogen phase diagram was to determine the liquidus and solidus lines as a function of hydrogen partial pressure. For this measurement, a special differential thermal analysis (DTA) unit was used. Sample sizes of 15g were used for analysis. The tests were conducted with a molybdenum reference standard and the heating and cooling rate was maintained at 0.6°C/s. Sample temperatures were measured by W-5%Re/W-20%Re thermocouples coated with a thin layer of alumina paint to prevent chemical reaction with the melt. The cold junction was maintained in ice water. Unlike most DTA tests, following vacuum evacuation, argon backfill, and a final vacuum evacuation, the test unit was pressurized with hydrogen at 0.18, 0.5, 1.0, 1.5 and 2.0 MPa. Several replicates were run under each condition (13 to 25 per point). The resultant liquidus and solidus curves for Alloy 625 measured by these experiments are shown in Figure 2.

Next, it was necessary to determine the amount of time necessary to allow for equilibration of dissolved hydrogen with the hydrogen gas present above the alloy. If the reaction to be studied is[2]

$$H_2 = 2\,\underline{H} \qquad (1)$$

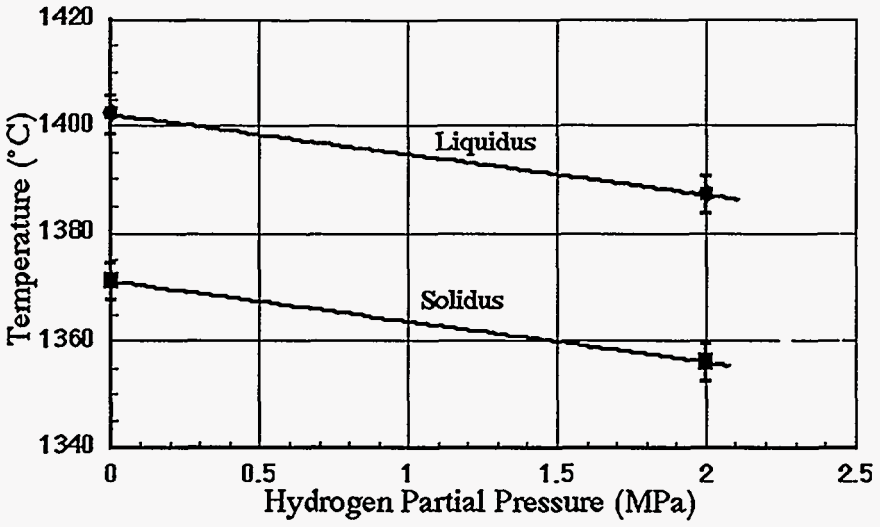

Figure 2. Liquidus and solidus curves for Alloy 625 in contact with hydrogen at varying pressures. Data points for pressure extremes are shown to illustrate statistical relevance of the data.

where $\underline{H}$ is the dissolved monatomic hydrogen in the sample. If p_{H_2} is the partial pressure of hydrogen gas circumjacent to the sample, the equilibrium constant can then be written as

$$K = \frac{a_{\underline{H}}^2}{p_{H_2}} \tag{2}$$

where a is the activity.

If one expects that hydrogen content dissolved in the liquid or solid will follow Henrian behavior, then

$$X_{\underline{H}} = \frac{K^{1/2}}{\gamma_{\underline{H}}} p_{H_2}^{1/2} \tag{3}$$

This well known relationship, Sievert's Law, shows that the dissolved hydrogen content, $X_{\underline{H}}$, should follow a parabolic relationship with the hydrogen partial pressure over the sample, assuming a constant activity coefficient $\gamma_{\underline{H}}$.

However, equilibration of dissolved hydrogen in the melt is dependent on time. For the lowest temperature investigated in the phase diagram analysis (1200°C), and at the lowest pressure of hydrogen that the samples were exposed to (0.1 MPa), experiments were conducted to determine the amount of time required to allow the samples to reach equilibrium hydrogen concentrations. The particular test apparatus consisted of a resistance heated furnace capable of being rotated 90°. A sample of approximately 4.3 g was placed in the furnace, the furnace was sealed, purged with inert gas, and backfilled with hydrogen gas to 0.1 MPa. The specimen was then heated to 1200°C and held for 5 to 100 min. The sample was then abruptly dropped into a water quench area inside the chamber by rotating the chamber 90°.

Hydrogen content in the sample was then measured by removing it from the chamber, drying it, and measuring the absorbed hydrogen. The measurement procedure involved placing the sample in a chamber of precisely known volume, evacuating the chamber to very low vacuum levels, isolating the chamber from the vacuum system, then heating the sample up to temperatures below 800°C to allow the dissolved hydrogen to bake out. By measuring the pressure in the chamber, and knowing its volume, the amount of hydrogen evolved can be calculated. This measurement procedure will hereafter be referred to as the bake-out measurement.

The results of these equilibration experiments for Alloy 625 are shown in Figure 3. As can be seen in the figure, the samples showed markedly different behavior depending on the

condition of the surface. As they emerged from the saturation furnace, the samples were covered with an adherent film. If the film was removed by hand grinding on emery paper, the saturation kinetics were straightforwardly measured and interpreted. If, however, this film remained on the sample during the bake-out step to measure dissolved hydrogen, the results were erratic. It was clear that the presence of this film retarded the ability of the hydrogen to diffuse from the samples during the bake out. However, this film obviously did not interfere with the saturation of hydrogen in the furnace, either because it was not present until after the melting was completed, or because the higher temperatures allowed hydrogen diffusion rates that overwhelmed the effect of any film.

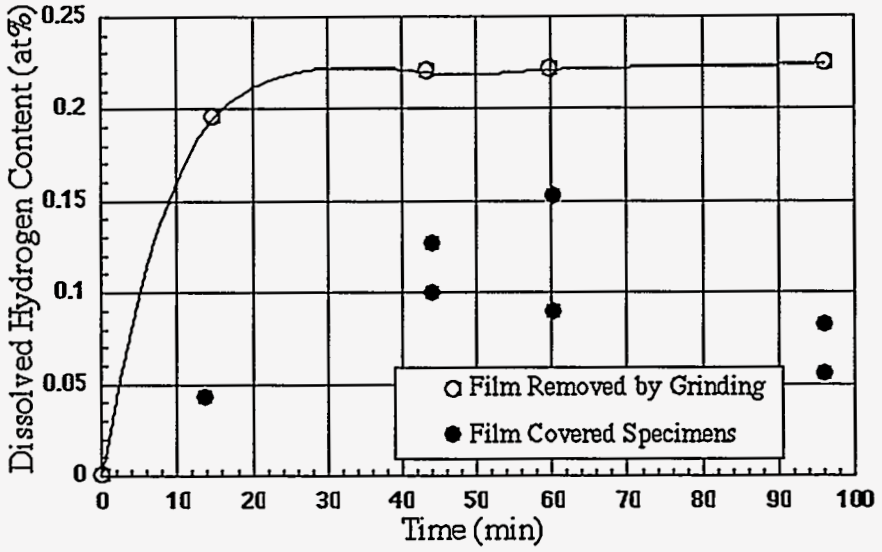

Figure 3. Saturation of hydrogen in Alloy 625 as a function of time for p_{H_2} = 0.1 MPa.

Next, hydrogen solubility was measured for several temperatures in both liquid and solid Alloy 625. Saturation of hydrogen in the solid was measured at 1200, 1250, 1300, and 1350°C, while saturation in the liquid was measured at 1450, 1500, and 1550°C. Hydrogen gas pressures of 0.18, 0.5, 1.0, 1.5 and 2.0 MPa were used. In the case of samples saturated with hydrogen in the solid state, the procedure was very similar to that described for the saturation time study described above. However, for the samples saturated with hydrogen in the liquid state, quenching in water would be dangerous. Moreover, since gas pores are generated during solidification, a certain amount of hydrogen gas would escape from the pores, and the amount of dissolved hydrogen that was present in the liquid would not be accurately reflected in the bake-out measurements. In order to suppress pore formation, once saturated, the melting chamber was then overpressurized to a total of 4 MPa with argon gas and subsequently quenched into a copper crucible. The argon overpressure suppressed any pores, and retained the soluble hydrogen in the solid samples so they could be analyzed with bake-out measurements.

The summary data for hydrogen solubility in solid and liquid Alloy 625 are shown in Figure 4. As one would expect, the higher the temperature, the greater the amount of hydrogen that is soluble in either the liquid or the solid. To verify if Sievert's law was being obeyed, a plot of hydrogen solubility as a function of $\left(p_{H_2}\right)^{1/2}$ was used to check for linearity. As can be seen in Figure 5, Sievert's law is in fact obeyed quite well. In fact, this adherence to Sievert's law held for all of the alloys. The effect of temperature on the solubility of hydrogen can also be determined from[3]

$$X_{\underline{H}} = A\exp\left(-\frac{\Delta\overline{H}_H}{2RT}\right)p_{H_2}^{1/2} \qquad (4)$$

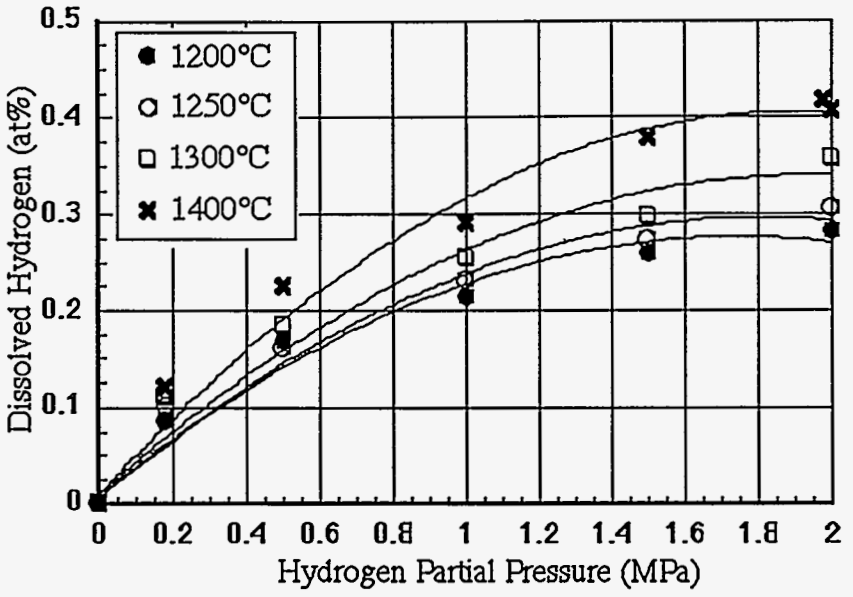

(a)

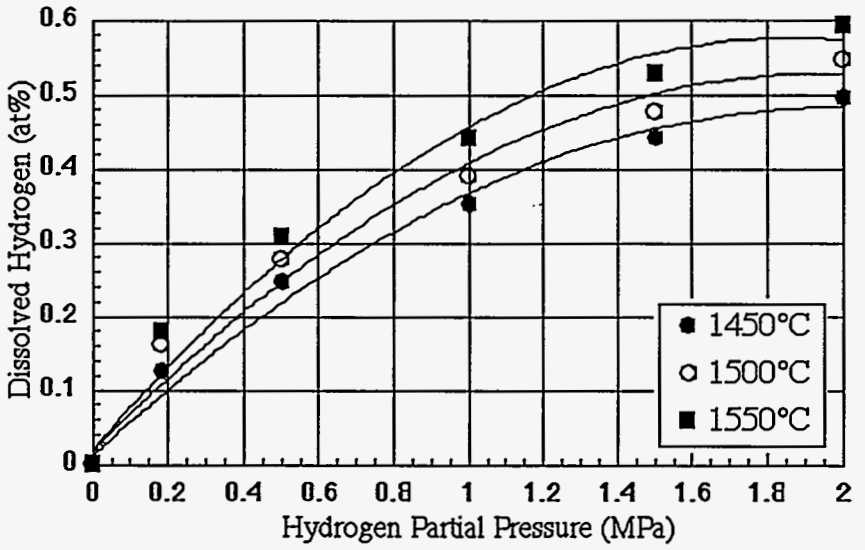

(b)

Figure 4. Solubility of hydrogen in Alloy 625 in the (a) solid and (b) liquid.

Hence with an Arrhenius analysis of the data one can determine the enthalpy of solution, $\Delta\overline{H_H}$, of hydrogen in either the liquid or solid alloy. The enthalpies of solution for hydrogen, $\Delta\overline{H_H}$, are shown in Table 2.

Table 2. Enthalpies of Solution for Alloys in this Study
(standard deviation shown in parentheses)

Alloy	$\Delta\overline{H_H}$, solid kJ/mol	$\Delta\overline{H_H}$, liquid kJ/mol
Alloy 625	74.3 (19.1)	112 (22.6)
Alloy 718	46.6 (26.1)	85.0 (17)
PH13-8Mo	75.2 (18.6)	84.3 (20.6)
ASTM F-75	87.4 (21.1)	76.2 (12.6)

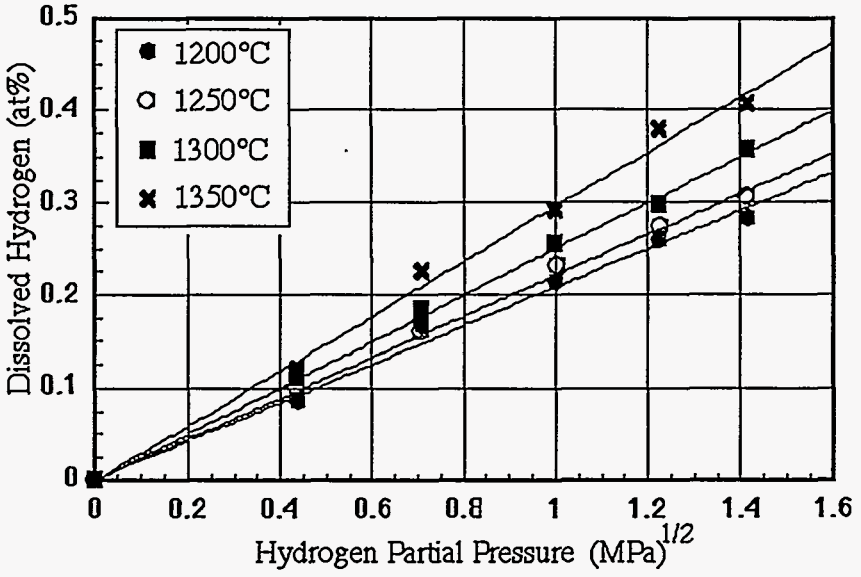

Figure 5. Data for Alloy 625 from Figure 4(a) replotted as a function of $\left(p_{H_2}\right)^{1/2}$ demonstrating conformance to Sievert's Law.

The summary phase diagram for Alloy 625 is shown are Figure 6(a). The phase diagram only contains the phase boundaries for a p_{H_2}=2.0 MPa. Although comparison to binary eutectic systems is not completely accurate, one can think of the point labeled "E" in Figure 6(a) as analogous to the eutectic point in binary systems. Completion of phase saturation kinetics, liquidus/solidus determination, and hydrogen solubility for the remainder of the alloys was also conducted. These data are omitted for brevity, but the summary phase diagrams at p_{H_2}=2.0 MPa are also included in Figure 6.

Based on prior development of the process in the former Soviet Union, an alloy's tendency for Gasar formation can be estimated by the discontinuity between hydrogen solubility in the liquid and the solid. Past experience has shown that this difference should roughly be 15%. While the absolute amount of the difference influences the amount of hydrogen released, hence the pore volume that can be generated, experience with this process has shown that this 15% difference is just an estimate of the suitability for Gasar formation. Figure 6 shows phase diagrams at the highest hydrogen pressure investigated, 2.0 MPa. This pressure showed the greatest difference in solubility of dissolved hydrogen between the liquid and the solid relative to lower hydrogen pressures. Therefore, one would expect that the tendency to produce Gasar structures could be enhanced at higher hydrogen pressures. Table 3 shows the calculated percentage changes in hydrogen solubility across the melting temperature range. Based on these observations, alloys like ASTM F-75 and Alloy 718 should be good candidates for Gasar formation, while the remaining alloys may not be as promising.

Table 3. Hydrogen Solubility Changes for Alloys
(p_{H_2} = 2.0 MPa)

Alloy	Percent Difference in Hydrogen Solubility Across Solidification Range	Other Observations
ASTM F-75	40	Large pores
Alloy 718	24	
Alloy 625	10	
PH13-8Mo	18	Strong film former on melt

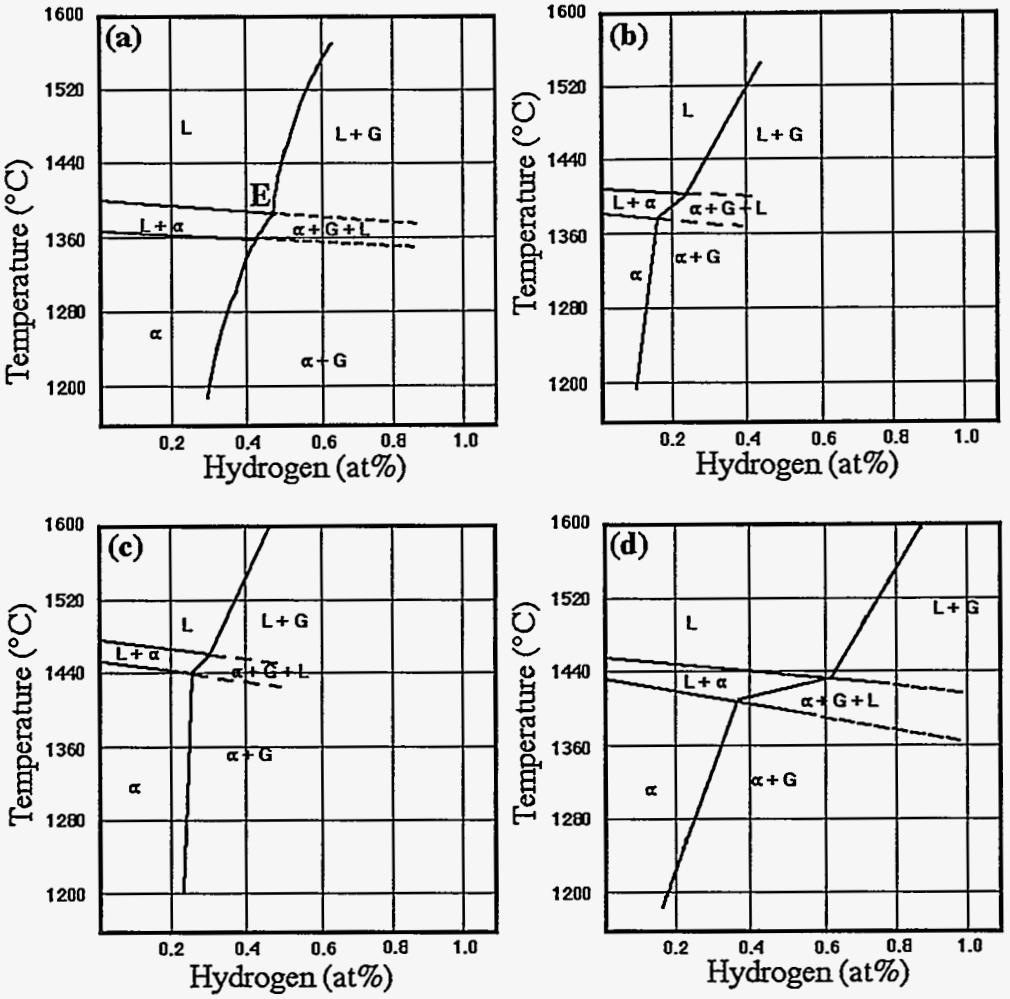

Figure 6. Selected high temperature alloy/hydrogen phase diagrams for (a) Alloy 625, (b) Alloy 718, (c) PH13-8Mo, and (d) ASTM F-75. All phase diagrams are for a $\left(p_{H_2}\right)^{1/2}$ of 2 MPa.

Sandia Gasar Furnace

The furnace constructed at Sandia National Laboratories for preparation of Gasar structures, shown in Figure 7, consists of a bottom-pour induction furnace housed inside an ASME certified pressure vessel. The empty volume of the furnace is 0.85 m^3. The vessel is water jacketed and rated for a maximum allowable working pressure of 800 psig. The vessel is constructed to allow both the top and bottom covers to be removed for access to the furnace coil and crucible from above, and to allow for access to the mold area in the bottom cover. The top cover contains the actuator for the crucible stopper rod and sight ports for viewing cameras and pyrometers. The bottom cover contains penetrations for instrumentation (camera, thermocouples, resistance heaters) as well as a separate cooling circuit for the mold area. The induction coil and crucible are held in place by a stainless steel plate supported on the sides of the vessel. The plate holds a large ceramic cylinder upon which the coil and crucible are held. Unlike more common vacuum furnaces, the feed-throughs for the coil are designed to withstand both vacuum evacuation and the rated pressure inside the vessel. A mechanical vane pump and diffusion pump combination are used to evacuate the chamber through a port opposite from the coil feed-throughs.

The molds for casting are designed to promote unidirectional solidification in either the vertical direction (axial solidification in a cylindrical casting), or in the radial direction

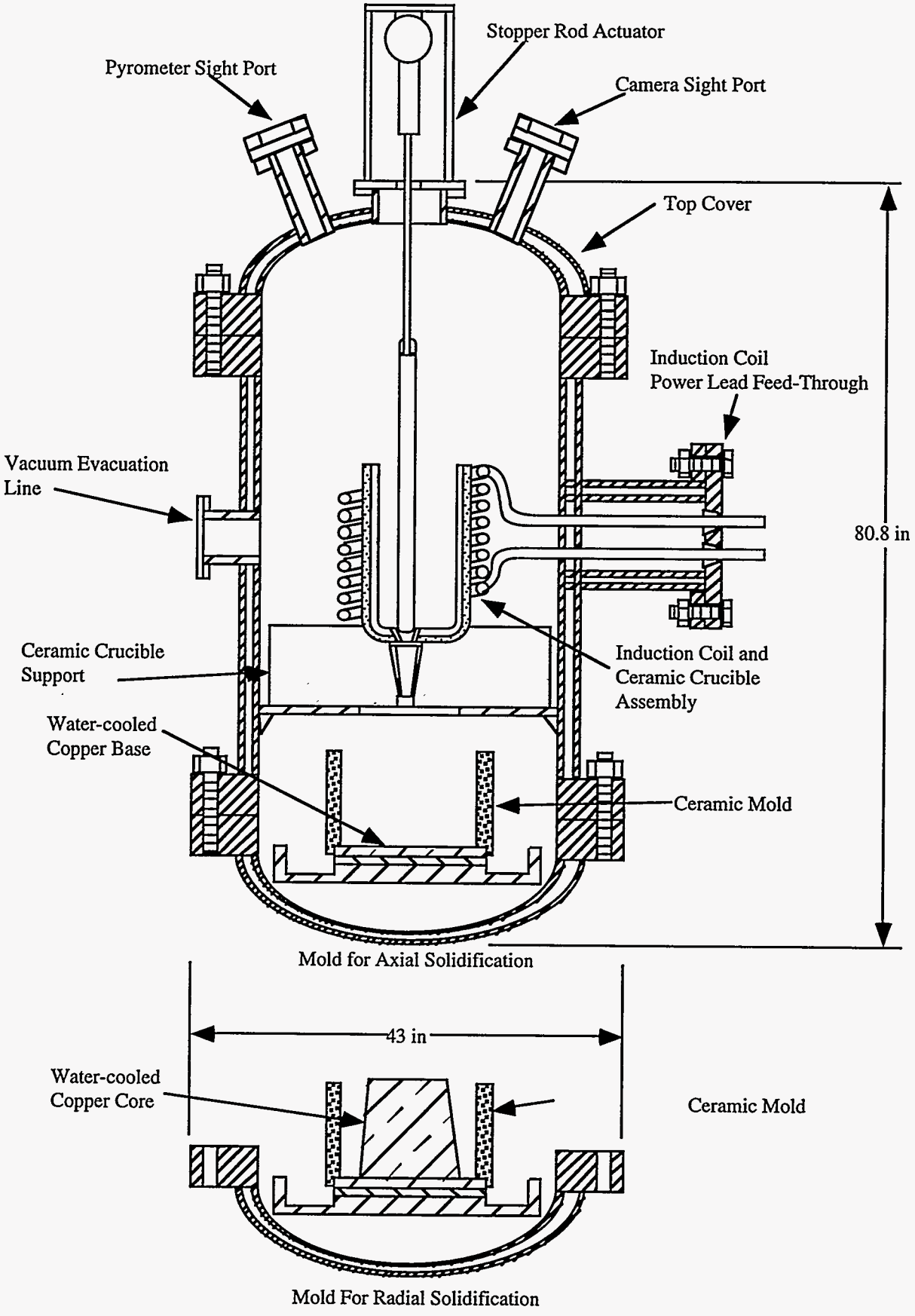

Figure 7. Schematic design of the Sandia Gasar furnace.

(solidification from the inner diameter to the outer diameter of a ring). Either mold can be placed in the bottom cover.

While the details of the operation of this furnace are beyond the scope of this paper, a summary of the general operational principles is rather simple. First, the metal charge and mold are put in place in the crucible and bottom cover, respectively. The bottom and top covers are installed and sealed, followed by vacuum evacuation of the chamber to 10^{-3} torr. The chamber is isolated from the vacuum pumps, an inert gas backfill is completed to about 1 atm, then the chamber is evacuated again. At this point the induction melting power supply can be activated. Depending on the material being melted, the furnace may also operate under inert gas at this point as well. Once the material has fully melted, the appropriate hydrogen gas mixture is introduced into the furnace. The melting is continued until the appropriate superheat and exposure time to absorb hydrogen has been reached. The metal is then tapped by lifting the stopper rod. Solidification commences when the metal reaches the water-cooled copper base-plate (or core). Once the chamber has cooled, the hydrogen gas mixture is vented, the chamber is purged with inert gas, vented again, and then opened.

Summary and Conclusions

Gasar materials represent an entirely new class of porous metal structures. The successful application and commercialization of these materials in the West depends on careful integration of former Soviet technology with the resources available in the U.S. This initial work, while focused on only a few alloys has shown that the proper metallurgical basis exists for Gasar formation for a few of these alloys. Of the four alloys chosen for investigation, Alloy 718 and ASTM F-75 appear to be the most promising for preparation of Gasar structures. The phase diagram determination for these alloys shows that the proper amount of hydrogen solubility mismatch between the liquid and the solid alloys exists over the melting range. Future work with these alloys and the Gasar furnace at Sandia will study the porous structure of these alloys, in addition to others.

Acknowledgments

Technical assistance from Marina Vlasova and Vladimir Karpov at SMA of Ukraine is greatly appreciated. Thanks are also owed to Matthew Walukas and Vladimir Polskii of DMK Tek for their translation assistance during the early portion of this work. Special consideration also goes to Thomas Gutsch, Mark Miszkiel, and Dave Schmale for tireless efforts to bring the Sandia Gasar furnace to completion. This work was supported by the United States Department of Energy under Contract DE-AC04-94AL85000. Sandia is a multiprogram laboratory operated by Sandia Corporation, a Lockheed Martin Company, for the United States Department of Energy.

References

1. V. Shapovalov, "Porous Metals", MRS Bulletin, v. XIX, No. 4, 24-28.
2. V.I. Shapovalov, U.S. Patent No 5,181,549, (January 26, 1993)
3. R.A. Swalin, Thermodynamics of Solids, 2nd Ed., John Wiley and Sons, New York, NY, p.177-178 (1972).